



Boussinesq evolution equations: numerical efficiency, breaking and amplitude dispersion

H. Bredmose^{a,*}, H.A. Schäffer^b, P.A. Madsen^a

^a*Department of Mechanical Engineering, Technical University of Denmark, Building 403, Lyngby DK-2800, Denmark*

^b*DHI Water & Environment, Agern Allé 5, Hørsholm DK-2970, Denmark*

Received 12 May 2003; received in revised form 17 June 2004; accepted 21 July 2004

Available online 15 September 2004

Abstract

This paper deals with the possibility of using methods and ideas from time domain Boussinesq formulations in the corresponding frequency domain formulations. We term such frequency domain models “evolution equations”. First, we demonstrate that the numerical efficiency of the deterministic Boussinesq evolution equations of Madsen and Sørensen [Madsen, P.A., Sørensen, O.R., 1993. Bound waves and triad interactions in shallow water. *Ocean Eng.* 20 359–388] can be improved by using Fast Fourier Transforms to evaluate the nonlinear terms. For a practical example of irregular waves propagating over a submerged bar, it is demonstrated that evolution equations utilising FFT can be solved around 100 times faster than the corresponding time domain model. Use of FFT provides an efficient bridge between the frequency domain and the time domain. We utilise this by adapting the surface roller model for wave breaking to frequency domain evolution equations. An equation for the variation of the mean water level is derived. Results for regular and irregular waves are presented and compared to results of conventional breaking formulations for evolution equations as well as for results of the corresponding time domain model. Emphasis is given to the shape of the breaking waves. The amplitude dispersion of evolution equations is analysed using a third-order perturbation approach. It is found to exceed the amplitude dispersion of the corresponding time domain model, and the approximation causing this deviation is pinpointed.

© 2004 Elsevier B.V. All rights reserved.

Keywords: Frequency domain modelling; Deterministic modelling; Computational efficiency; Wave breaking; Irregular waves; Roller model; Boussinesq models; Amplitude dispersion

1. Introduction

Wave trains propagating from deep water towards the shore are subject to the processes of shoaling, refraction and nonlinear interactions. Boussinesq models are often chosen as modelling tool for such situations. For wave fields of two horizontal dimen-

* Corresponding author. Now at School of Mathematics, University of Bristol, University Walk, Bristol BS8 1TW, United Kingdom.

E-mail address: h.bredmose@bristol.ac.uk (H. Bredmose).

sions, the computational costs of solving a Boussinesq model can still be substantial. If the wave field is weakly nonlinear, the depth varies slowly in space and reflection is negligible, the corresponding frequency domain formulations provide a simpler and computationally cheaper method for calculating the evolution of the wave field. We term such models *evolution equations* throughout this paper.

Evolution equations are derived by expanding the flow variables as Fourier series. By inserting these expansions into the governing time domain equations, the time is eliminated as independent variable, and a system of equations in the spatial variation of the Fourier amplitudes is obtained. If the phases of the Fourier amplitudes are included in the model, we term the model deterministic. Deterministic models may be manipulated further to remove the phases, thus leading to stochastic models (e.g. Herbers and Burton, 1997; Agnon and Sheremet, 1997). All evolution equations considered in this paper are deterministic, and for simplicity we consider only models for wave fields of one horizontal dimension.

Boussinesq formulations have often been used as the starting point for the derivation of evolution equations, since they offer a depth-integrated form of the governing equations. Evolution equations based on the classical Boussinesq equations of Peregrine (1967) have been addressed by Mei and Ünlüata (1972), Freilich and Guza (1984), Liu et al. (1985) among others. Starting in the early 1990s, a series of time domain Boussinesq formulations appeared, with improved linear and nonlinear characteristics (e.g. Madsen and Sørensen, 1992; Nwogu, 1993; Wei et al., 1995; Madsen and Schäffer, 1998; Gobbi et al., 2000; Kennedy et al., 2001; Madsen et al., 2002). This initiated the development of new evolution equation models. Madsen and Sørensen (1993) derived one-dimensional evolution equations based on the Boussinesq formulation of Madsen and Sørensen (1992) and Chen and Liu (1995) and Kaihatu and Kirby (1998) derived evolution equations based on the Boussinesq formulation of Nwogu (1993).

Usually, evolution equations require a computational effort of $O(N^2)$, where N is the number of frequencies treated. This makes evolution equations unattractive for simulating irregular sea states with a large number of frequencies. However, the computational effort can be reduced to $O(N \log N)$ utilising the

Fast Fourier Transform algorithm (FFT). In this paper, we demonstrate how this technique can be used, thus widening the applicability range of evolution equations. We present a comparison of the computational efficiency of the time domain model of Madsen and Sørensen (1992) and the corresponding evolution equations of Madsen and Sørensen (1993) utilising FFT. For the specific physical test chosen, nonbreaking irregular waves passing a bar, the evolution equations are found to require 100 times less CPU-time than the time domain model.

The availability of FFT to toggle efficiently between the frequency domain and the time domain makes it possible to incorporate ideas and methods successfully used in the time domain into the frequency domain models. We exploit this idea here by adapting the surface roller breaking model, which has been successfully used in the time domain (Schäffer et al., 1993; Madsen et al., 1997a,b), to the frequency domain.

Traditionally, wave breaking is described by incorporating an additional quasi-linear damping term into the equations. The total decrease in energy flux due to wave breaking is determined using an empirical dissipation model, and is then distributed among the frequencies according to a chosen weighting. The damping coefficient is usually taken to be real, and thereby any phase effects of the breaking are discarded. Further, the dissipation due to breaking is induced globally on the spectrum and does not take basis in the individual physical breaking events. Using a time series-based breaking formulation may improve on these points. We test this hypothesis by comparing results of the new roller breaking formulation to results of the breaking model of Eldeberky and Battjes (1996).

Because the phases of the wave amplitudes are included in the modelling, time series in any location are readily available by the aid of FFT. We therefore find it natural to base the judgement of the model results on actual time series, rather than on plots of power spectra and global measures such as skewness and asymmetry. This view also yields insight into the question, if the quality of time series obtained by evolution equations matches the quality of time series from the corresponding time domain model. We address this question by comparing time series for breaking wave results of the Boussinesq model of Madsen et al. (1997a) and the corresponding evolution

equations of Madsen and Sørensen (1993) extended with roller breaking.

The last part of the paper deals with the amplitude dispersion of the evolution equations of Madsen and Sørensen (1993). The comparison of breaking waves results of this model to results of the corresponding time domain model suggest that the amplitude dispersion is stronger for the evolution equations. We thus present a Stokes-type third-order perturbation analysis, confirming this observation and pinpointing which step in the derivation of the evolution equations is the main cause.

The outline of the paper is as follows. In Section 2, the derivation of the evolution equations of Madsen and Sørensen (1993) is summarised. The speed-up technique of using FFT and the comparison of computational efficiency is presented in Section 3. Section 4 opens with a review of breaking formulations in the frequency domain and time domain and then describes the adaption of the roller breaking model into evolution equations. The treatment of mean water level variation is presented as well. In Section 5, results for regular waves are presented, while results for irregular waves breaking over a submerged bar are given in Section 6. Finally, in Section 7, the analysis of amplitude dispersion is given.

2. The evolution equations of Madsen and Sørensen (1993)

The deterministic evolution equations of Madsen and Sørensen (1993) are based on a time domain Boussinesq formulation in the free surface elevation η and the depth-integrated velocity P . For one horizontal dimension, the time domain equations read

$$\eta_t + P_x = 0 \tag{2.1}$$

$$P_t + \left(\frac{P^2}{h + \eta} \right)_x + g(h + \eta)\eta_x - Bgh^3\eta_{xxx} - (B + 1/3)h^2P_{xxt} - h_x \left(2Bgh^2\eta_{xx} + \frac{1}{3}hP_{xt} \right) = 0, \tag{2.2}$$

where η is measured upwards from the still water level, h is the undisturbed depth and g is the

acceleration of gravity. B is a free parameter governing the linear dispersion properties of the equation. For $B=1/15$, the Padé [2,2]-dispersion relation is achieved. The model is valid for slowly varying depth. Eqs. (2.1) and (2.2) describe the conservation of mass and momentum, respectively.

2.1. Transformation to the frequency domain

To derive deterministic evolution equations based on Eqs. (2.1) and (2.2), Madsen and Sørensen (1993) eliminated P in the linear terms by cross-differentiation. They hereby obtained the wave equation

$$\begin{aligned} \eta_{tt} - g\eta_{xx} + Bgh^3\eta_{xxxx} - (B + 1/3)h^2\eta_{xxt} \\ - (g\eta_x + (2B + 1)h\eta_{xt} - 5Bgh^2\eta_{xxx})h_x \\ = \left(\frac{1}{2}g\eta^2 + \frac{P^2}{h + \eta} \right)_{xx} \end{aligned} \tag{2.3}$$

where the terms in the first line are the linear terms, and the terms in the second and third line are the bottom slope terms and the nonlinear terms, respectively. To derive this equation, only the lowest-order terms in h_x were retained.

Next, the following series for η and P were substituted

$$\begin{aligned} \eta(x, t) &= \sum_{p=-N}^N a_p(x) e^{i(\omega_p t - \int k_p dx)}; \\ P(x, t) &= \sum_{p=-N}^N b_p(x) e^{i(\omega_p t - \int k_p dx)}, \end{aligned} \tag{2.4}$$

where $\omega_p = p\omega_1$, $(a, b)_{-p} = (a^*, b^*)_p$ and (a_0, b_0) are real. Evaluation of all the derivatives and collection of terms lead to

$$\begin{aligned} \beta_{4,p}a_{p,xxxx} - i\beta_{3,p}a_{p,xxx} - \beta_{2,p}a_{p,xx} + i\beta_{1,p}a_{p,x} \\ + i\beta_{1,p}\beta_{s,p}\frac{h_x}{h}a_p + \beta_{0,p}a_p = -\hat{\mathcal{N}}_{p,xx}e^{i\int k_p dx} \end{aligned} \tag{2.5}$$

for $p=1, \dots, N$, where \hat{N}_p is the p th Fourier component of the nonlinear term, defined through the Fourier transform

$$\frac{1}{2}g\eta^2 + \frac{P^2}{h + \eta} \equiv \sum_{m=-\infty}^{\infty} \hat{N}_m e^{im\omega t}. \quad (2.6)$$

The β -coefficients were given by

$$\beta_{4,p} = -Bgh^3 \quad (2.7a)$$

$$\beta_{3,p} = -4Bgh^3 k_p \quad (2.7b)$$

$$\beta_{2,p} = -\left(gh + 6Bgh^3 k_p^2 - (B + 1/3)h^2 \omega_p^2\right) \quad (2.7c)$$

$$\beta_{1,p} = -2\left(ghk_p + 2Bgh^3 k_p^3 - (B + 1/3)h^2 \omega_p^2 k_p\right) \quad (2.7d)$$

$$\beta_{0,p} = \omega_p^2 - ghk_p^2 - Bgh^3 k_p^4 + (B + 1/3)h^2 \omega_p^2 k_p^2 \quad (2.7e)$$

$$\begin{aligned} \beta_{s,p} = & \left(1 + (4B - 1)k_p^2 h^2 + \left(6B^2 - \frac{2}{3}B\right)k_p^4 h^4\right. \\ & + \left(4B^3 + \frac{1}{3}B^2 + \frac{1}{9}\right)k_p^6 h^6 \\ & + \left(B^4 - \frac{1}{9}B^2\right)k_p^8 h^8 \\ & \left. / \left(4\left(1 + 2Bk_p^2 h^2 + \left(B^2 + \frac{1}{3}B\right)k_p^4 h^4\right)^2\right) \right) \end{aligned} \quad (2.7f)$$

We note that the equation $\beta_{0,p}=0$ establishes the linear dispersion relation of the wave model. In the following we let k_p be the free wave number at frequency p , such that $\beta_{0,p}=0$ throughout.

Madsen and Sørensen (1993) applied four approximations to derive evolution equations from the above equations. The approximations were all motivated by the assumption of slowly varying

depth and weak nonlinearity leading to slowly varying wave amplitudes. The approximations are:

- (I) rewriting of the nonlinear term $P^2/(h+\eta)$ to P^2/h
- (II) neglect of higher-order linear derivatives of $a_p(x)$, such that only $a_{p,x}$ is retained
- (III) a linear approximation for the flux amplitudes in the nonlinear term $b_p = \omega_p a_p / k_p$ and
- (IV) neglect of derivatives of $a_p(x)$ and $h(x)$ in the nonlinear terms.

With these four approximations, Madsen and Sørensen (1993) obtained the evolution equations

$$\begin{aligned} a_{p,x} = & -\beta_{s,p} \frac{h_x}{h} a_p - \frac{i}{\beta_{1,p}} g \sum_{s=p-N}^N (k_s + k_{p-s})^2 \\ & \times \left(\frac{1}{2} + \frac{1}{gh} \frac{\omega_s \omega_{p-s}}{k_s k_{p-s}}\right) a_s a_{p-s} e^{-i \int (k_s + k_{p-s} - k_p) dx} \end{aligned} \quad (2.8)$$

for $p=1, \dots, N$.

3. Improvement of efficiency using the FFT algorithm

Straightforward solution of the model (Eq. (2.8)) requires a computational effort of $O(N^2)$ due to the summations involved. This makes evolution equations like Eq. (2.8) impractical for wave spectra involving a large number of frequencies, corresponding to long time series. However, within spectral methods for partial differential equations, sums of the above type have been recognized as convolution sums. As such, they can be handled with a computational effort of $O(N \log N)$ using the convolution theorem and the Fast Fourier Transform algorithm (FFT). This technique was developed independently by Orszag (1969, 1970) and Eliassen et al. (1970) (see Canuto et al., 1987). Fornberg and Whitham (1978) used a variant of this method for time stepping the Korteweg–de Vries equation. However, within the field of spatial wave evolution equations, the speed-up technique of applying FFT to the

nonlinear terms does not seem to have been used before.

The concept of using FFT is straightforward. Combining Eqs. (2.5) and (2.8), we see that the evolution equations can be written in the alternative form

$$a_{p,x} = -\beta_{s,p} \frac{h_x}{h} a_p + \frac{i}{\beta_{1,p}} \hat{N}_{p,xx} e^{i \int k_p dx}. \quad (3.1)$$

Hence, the convolution sum in Eq. (2.8) is nothing but the p th Fourier coefficient of the time series $((1/2)g\eta^2 + P^2/h)_{xx}$ multiplied by $ie^{i \int k_p dx} / \beta_{1,p}$. As an alternative to the convolution approach, one may therefore construct this time series explicitly and transform it back to the frequency domain using forward FFT. To calculate the time series, we first expand the double x -differentiation, ignoring the spatial variation of h

$$\left(\frac{1}{2}g\eta^2 + \frac{P^2}{h} \right)_{xx} = g(\eta_{xx} + \eta_x^2) + \frac{2}{h}(PP_{xx} + P_x^2). \quad (3.2)$$

Time series for η , η_x , η_{xx} , P , P_x and P_{xx} are obtained by backward FFTs of their Fourier coefficients, obtained from the complex wave amplitudes $a_{1,\dots,N}$. The derivatives are calculated spectrally by multiplying the Fourier coefficients by $-ik_p$ and $-k_p^2$, respectively, while the Fourier coefficients of the flux, P , are calculated using the linear approximation $b_p = (\omega_p/k_p)a_p$. This corresponds to the approximations (I)–(IV) of Section 2.

Once the time series for η , η_x , η_{xx} , P , P_x and P_{xx} are obtained, the product (Eq. (3.2)) can be calculated as a time series and transformed back to the frequency domain by forward FFT. The resulting Fourier coefficients are inserted into Eq. (3.1), thereby providing the nonlinear term at a cost of $O(N \log N)$. The results of using Eq. (3.1) are identical to the results of Eq. (2.8) to machine accuracy.

3.1. Avoidance of aliasing

When calculating the nonlinear term, a sufficient number of discrete points in the time series must be

involved to avoid aliasing. The surface elevation η is described by N positive frequencies, the largest being denoted f_N . A quadratic product of η will have a maximum frequency of $2f_N$, and therefore requires a minimum of $4N$ points to be properly resolved. However, since we only need the first N Fourier coefficients of the quadratic time series (Eq. (3.2)), corresponding to the frequencies of the wave amplitudes $a_{1,\dots,N}$, $3N+1$ time series points are sufficient. More details on this can be found in Canuto et al. (1987).

3.2. A practical comparison of CPU-times

With the above speed-up, an irregular wave field of N positive frequencies in a domain of Q spatial points can be calculated with a computational effort of $O(QN \log N)$. In comparison to the traditional handling of evolution equations, implying a computational effort of $O(QN^2)$ this is a clear improvement. However, as time domain Boussinesq models can solve the same problem with an asymptotic work load of $O(QN)$, a practical investigation of the computational performance of evolution equations versus time domain models is motivated. Such a comparison is presented in the following, comparing the computational efficiency of the time domain model (Eqs. (2.1) and (2.2)) and the corresponding evolution equations (Eq. (2.8)).

As physical test case, we choose an irregular wave field of 800 frequencies, propagating over a submerged bar. The bar topography is shown in Fig. 1. In front of and behind the bar, the depth is 0.4 m, while on top of the bar the depth is 0.1 m. The upward slope is 1:20 and the downward slope is 1:10. The incoming wave spectrum is a JONSWAP spectrum with a peak period of 2.02 s and the largest frequency chosen as $f_{\max} = 4f_{\text{peak}}$. This implies that the largest error in the Padé[2,2] phase speed is 23%. This is a rather large error, and for practical use a smaller cutoff frequency is generally recommended. On the other hand, this error is valid for the deep parts of the domain, while for the shallow part of the domain, the largest error in phase speed is 0.4%. In the shallow part of the domain, high-frequency bound waves are expected. For this reason it was decided to retain this rather high cutoff frequency, although it can be argued that the high-frequency free waves are thus described inaccurately.

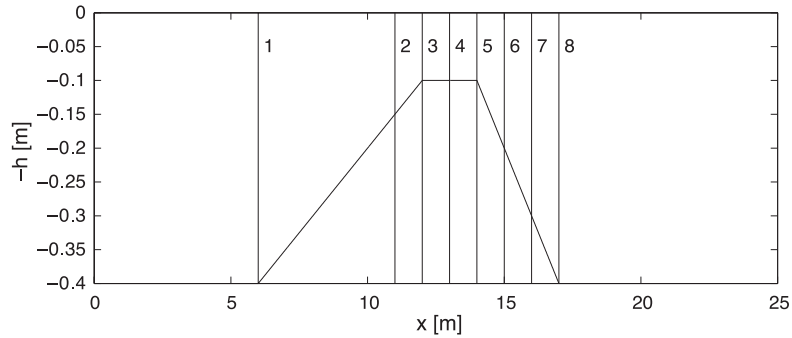


Fig. 1. Bathymetry for the test of irregular waves passing a submerged bar. The vertical lines mark the position of measurement stations, as referred to in Section 6.

ately. The chosen frequency resolution corresponds to a physical time series length of 200 peak periods, resolved with 1600 time steps. The significant wave height for the truncated spectrum is 3.63 cm. With this wave height the largest waves on the bar top are close to the limiting wave height for regular waves of the peak period.

Due to the approximations involved when transforming the time domain model to the evolution equations (Eq. (2.8)), it is not feasible to compare results of the two models directly. Even for the finest discretisation of each model, the results will differ, since the equations solved are not identical. Instead, another approach was taken: for each model, a number of runs were carried out with different discretisations. The results of the finest grid was regarded as the ‘true’ solution for each model, and thus used as a reference solution. For all other grids, the error measure

$$\text{Err}_{\text{time series}}(x) = \frac{\frac{1}{M} \sum_{j=1}^M |\eta_j - \eta_{\text{ref},j}|}{\frac{1}{M} \sum_{j=1}^M |\eta_{\text{ref},j}|} \quad (3.3)$$

was defined, where M is the number of points in the time series. The error measure is defined in each spatial point and can be interpreted as the mean absolute error, normalised by the mean absolute value of the reference time series. To describe the

deviation from the reference solution by one single number, the mean error

$$\text{Err}^* = \frac{1}{8} \sum_{x=17}^{24} \text{Err}_{\text{time series}}(x), \quad (3.4)$$

was defined, being the mean value of the time series errors on the flat bottom after the bar, taken over spatial points with a distance of 1 m. Using this single number from each run, a curve illustrating the accuracy as function of CPU-time can be obtained. The efficiency of the models can then be compared by comparing these curves.

Using this approach, results of the two models are never compared directly. This is appropriate since the models are not identical. On the other hand, if one of the models is much simpler than the other, it may show a fast convergence with small CPU-times, still producing a solution of low quality in a physical sense. The results of the present investigation therefore show how fast each model can be solved satisfactorily, once the user has accepted the approximations involved with the model.

3.2.1. Results

The frequency domain model was solved using a fourth-order Runge–Kutta type explicit scheme, which is due to [Scraton \(1964\)](#). The reason for not using a standard Runge–Kutta method is the following: When integrating the solution in the interval $x=[x_j; x_j+\Delta x]$, the standard Runge–Kutta method evaluates the right-hand side of the ODE-system in the points $(x_j, x_j+\Delta x/2, x_j+\Delta x)$. If $x_j+\Delta x$ is a corner

point of the bar, the solution in $x_j + \Delta x$ will be affected by the new bed slope of the corner point. The effect will be $O(\Delta x \Delta h_x)$, where Δh_x is the change in h_x over the corner point. Hereby, the fourth-order accuracy of the integration scheme is violated. Note that assigning the pre-corner value of the bed slope to the corner point does not solve the problem, but only moves it to the next grid point after the corner.

The method of Scraton evaluates the right-hand side in the points $(x_j, x_j + 2/9\Delta x, x_j + 1/3\Delta x, x_j + 3/4\Delta x, x_j + 9/10\Delta x)$. The right-hand side is thus not evaluated in the end point of the integration interval. This makes it possible to retain the fourth-order accuracy of the method, even though the bed slope is discontinuous in the domain.

In Fig. 2, the time series error (Eq. (3.3)) is plotted as function of space for the results of the frequency domain model. The model was run with step sizes varying between 1 m and 10^{-3} m, fixed for each run. Results of the latter resolution was used as reference solution.

The error decreases with decreasing grid spacing. For fixed grid spacing, the error increases most rapidly on top of the bar, where the nonlinear contribution to the wave evolution is largest. In the section of constant depth after the bar, the error is almost constant, implying that the error induced at the top of the bar is carried along in the remaining part of the domain.

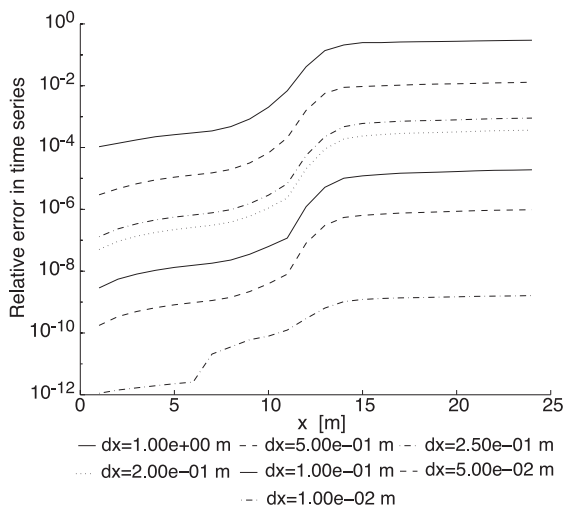


Fig. 2. Time series error as function of space for various step lengths.

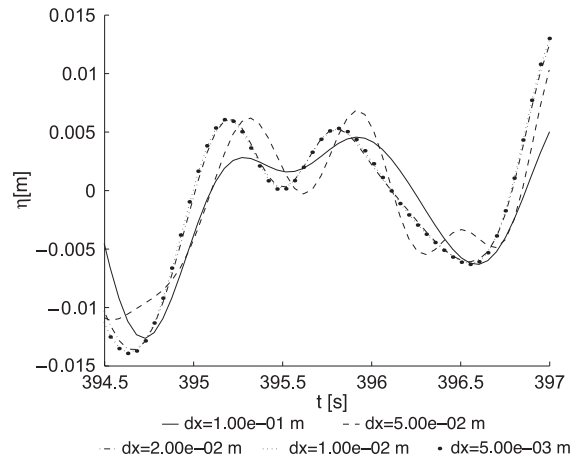


Fig. 3. Time series in $x=24$ m.

The time domain model was solved on the same computer, using a second-order finite difference scheme, staggered in space and time. The initial complex amplitude spectrum used for the evolution equations was transformed to a time series and used as the driving boundary condition in the time domain model. The length of this time series was 200 peak periods, and to warm up the computational domain, the last 40 peak periods of the time series were copied to the beginning of the signal. This results in a simulation length of 240 peak periods, for which the solution is periodic with a period of 200 peak periods. Only the last 200 peak periods were used in the post-processing. The incoming waves were generated internally in $x=5$ m, and sponge layers of 4 m length were incorporated in each end of the domain. The total length of the domain was 30 m.

Runs were carried out with grid spacings of $dx=(0.1, 0.05, 0.02, 0.01, 0.005)$ m, the latter being used as reference solution. The Courant number was chosen to be $C_r = \sqrt{gh}\Delta t/\Delta x = 0.40$ for all runs, determined at the depth of 0.4 m.

The variation of the time series error (Eq. (3.3)) is similar to the variation observed for the evolution equations of Fig. 2. In Fig. 3, a short section of the time series for η in $x=24$ m is shown for different grid spacings. We see that the use of a too coarse grid implies errors in the amplitude as well as the phase. The solution obtained with a grid spacing of 0.02 m has a value of Err^* of 9.7%. On the plot, it seems very close to the reference solution, thus indicating that Err^* is a rather hard error measure. This finding is

general for all the time series analysed, and we therefore judged that an error level of $Err^*=10\%$ is an acceptable requirement for solutions of practical quality.

For each run of the two models, the CPU-time was measured twice. The deviation between the two measurements of CPU-time was in general of the order $O(1\%)$. In Fig. 4, the values of Err^* are plotted as function of CPU-time for the two models. A straight line is fitted to the points in the double logarithmic plot. The different slopes of the lines are due to the different orders of accuracy for the numerical schemes used. The difference in CPU-time increases with increasing error level. For a time series error of 10%, the ratio between the CPU-times is 117. As mentioned, we consider this error level as a reasonable target for practical applications.

Obviously, the CPU-time is affected by a number of factors. The above test should therefore not be regarded as a precise estimate of the difference in CPU-times, since a factor of 2 or even 5 could easily enter the CPU-times obtained. Also, the above results are just for one single physical test. Nevertheless, the large ratio of about 100 clearly shows that evolution equations are indeed faster to solve than the corresponding time domain models. The main reason for this is the smaller need of spatial resolution for the evolution equations. While the time domain model must resolve the whole wave profile, the evolution equations only need to resolve the complex wave amplitudes, which vary slowly in space. Further, the requirement of a Courant number less than 1 for the time domain model enforces a much smaller time step, than needed for describing

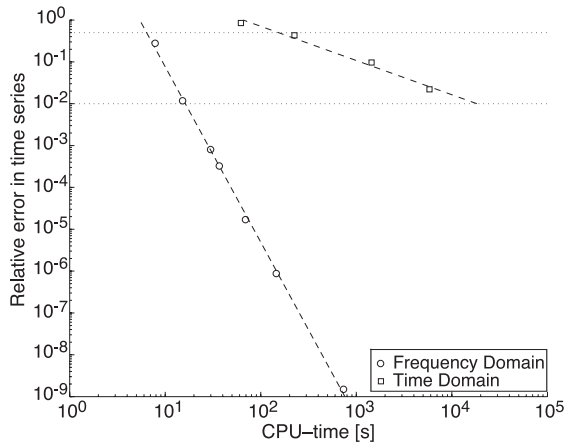


Fig. 4. Lines fitted through CPU-time results for irregular waves.

the cutoff frequency as a Nyquist wave. Within evolution equations, there is no coupling between the choice of spatial step and frequency resolution. Finally, no warm up time is needed for the evolution equations. For the present test, the warm up time chosen resulted in a 20% increase of the total simulation time. For regular waves, the ratio of warm up time to the total simulation time becomes very large.

Summarising, the above test indicates that evolution equations are much faster to solve than the corresponding time domain models. However, as the models are not identical, it is interesting to ask how much the results differ between the models. We get back to this issue in Sections 5 and 6.

4. Wave breaking in evolution equations

Using FFT to toggle between time series and complex wave spectra opens up the possibility of transferring methods and ideas from time domain Boussinesq formulations to their evolution equation counterparts. We here exploit this possibility by adopting the surface roller breaking concept into the evolution equations of Madsen and Sørensen (1993). This breaking model has been found to describe the wave shape and wave height decay of breaking waves with good accuracy (see Schäffer et al., 1993; Madsen et al., 1997a). Before describing the incorporation of the roller model into evolution equations, a review of breaking formulations in frequency domain and time domain is given.

4.1. Review of breaking formulations

4.1.1. Frequency domain breaking models

Traditionally, breaking in evolution equations is included through a quasi-linear damping term, simply added to the right-hand side of the model:

$$a_{p,x|\text{breaking}} = -\frac{1}{2} \frac{\sigma_p D}{\sum_{n=1}^N \sigma_n F_n} a_p, \quad p = 1, \dots, N. \tag{4.1}$$

Here D is the spatial decrease in total energy flux due to breaking, which must be supplied by an empirical

breaking formulation, and F_n is a linear estimate of the energy flux at frequency n . The energy dissipation is weighted by the weighting function σ_p .

Formulations of this kind have been used by several authors (Mase and Kirby, 1992; Kaihatu and Kirby, 1995; Eldeberky and Battjes, 1996). To calibrate σ_p , Mase and Kirby (1992) analysed laboratory data for a uniformly sloping beach. The analysis showed that σ_p is a growing function of frequency, and Mase and Kirby found that an f_p^2 dependence was reasonable (f is frequency). They therefore chose the weighting

$$\sigma_p = F + (1 - F) f_p^2 \frac{\sum_{n=1}^N |a_n|^2}{\sum_{n=1}^N f_p^2 |a_n|^2} \quad (4.2)$$

with $F=0.5$. $F=1$ corresponds to dissipating the energy flux proportionally to the energy flux content at each frequency.

A breaking scheme of the above type was incorporated in the evolution equations of Madsen and Sørensen (1993) by Eldeberky and Battjes (1996). They assumed a uniform distribution of σ_p , corresponding to $F=1$ in Eq. (4.2). The gradient of the energy flux was determined from the dissipation model of Battjes and Janssen (1978) for irregular waves. This model states that the spatial decay of energy flux due to breaking can be expressed as

$$D = \rho g \frac{\alpha}{4} f_c Q_b H_{\max}^2 \quad (4.3)$$

where α is a free parameter of order 1, f_c is a characteristic frequency, and H_{\max} is the maximum local wave height, estimated as $H_{\max} = \gamma h$, where $\gamma \in [0.6; 0.8]$ and h is the local depth. Q_b is the so-called fraction of broken waves, which is given by

$$\frac{1 - Q_b}{\ln Q_b} = - \left(\frac{H_{\text{rms}}}{H_{\max}} \right)^2. \quad (4.4)$$

Further details are given in Battjes and Janssen (1978).

4.1.2. Influence of breaking on skewness and asymmetry

The results of Eldeberky and Battjes (1996) suggest that a uniform distribution of the energy dissipation is

sufficient for modelling the power spectra of breaking irregular waves. On the other hand, Mase and Kirby (1992) found that a weighting with f^2 should be used. This discrepancy was investigated in detail by Chen et al. (1997), who incorporated a breaking model like Eq. (4.1) into the evolution equations of Chen and Liu (1995). Ten data sets obtained in the laboratory as well as in the field were modelled. The overall conclusion was that the shape of the power spectra is not sensitive to the spectral distribution of the breaking dissipation. The higher-order measures of skewness and asymmetry, however, are significantly improved by choosing $F=0$ in Eq. (4.2).

It may seem a little surprising that the spectral shape is unaffected by the frequency dependence of the breaking dissipation. As suggested by Chen et al. (1997), a possible explanation is that the nonlinear energy transfer rearranges the spectral energy content during wave breaking. This explanation is supported by the work of Elgar et al. (1997), who analysed field measurements of wave breaking. The frequency distribution of the dissipation due to wave breaking was found to be similar to the frequency distribution of the net effect of nonlinear energy exchange. This indicates that the nonlinear interactions restore the spectral energy content in the frequencies where dissipation occur. This is further supported by the findings of Herbers et al. (2000). However, even though the nonlinear interactions may compensate for a wrong distribution of the energy dissipation in a numerical model, this is expectedly not the case for the phases. This may explain that the higher-order measures of skewness and asymmetry are not well modelled for a uniform breaking distribution.

In this paper, we base the discussion of the wave shape on evaluation of actual time series of the waves, rather than on the derived statistical measures of skewness and asymmetry. We find that this gives a better physical interpretation of the results. Further, we find that time series provide a better material for investigating the ability of evolution equations to produce results of similar quality as time domain models.

4.1.3. Time domain breaking models

In time domain Boussinesq formulations, a number of breaking formulations exist. Several

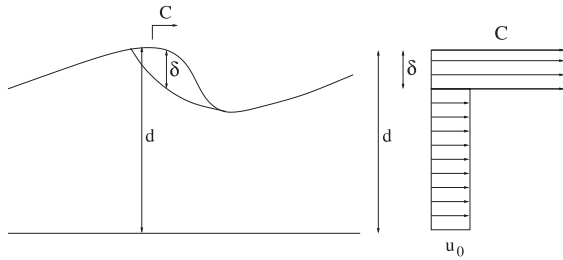


Fig. 5. Definition sketch and velocity profile for the roller model. The symbols are d =total water depth, c =wave speed, δ =roller thickness and u_0 =horizontal velocity below roller region.

authors (Tao, 1983; Abbott et al., 1983; Zelt, 1991; Sato et al., 1991; Karambas and Koutitas, 1992; Kennedy et al., 2000) have included the effect of wave breaking through an eddy-viscosity concept. In these works, the eddy viscosity formulation is based on horizontal gradients of the depth-integrated or depth-averaged horizontal velocity. Another approach is the incorporation of the surface roller concept, leading to an additional pressure term in the momentum equations (Deigaard, 1989; Brocchini et al., 1992) or an additional convective momentum term (Schäffer et al., 1993) in the momentum equations. Recently, Veeramony and Svendsen (2000) have presented a breaking model based on the vorticity generated by the breaking process.

Schäffer et al. (1993) applied their roller breaking model to regular and irregular waves breaking over a submerged bar. Further tests were presented by Madsen et al. (1997a) for uniformly sloping beaches. Since their Boussinesq model was only weakly nonlinear, the full wave height at the location of initial breaking was not reached for some of the tests. Apart from this, however, the model results for wave profiles and setup were in good agreement with measurements. Even the delayed onset of the setup just after the initiation of wave breaking is captured by the model. In a companion paper, Madsen et al. (1997b) presented results for irregular waves, including modelling of surf beat and run-up in the swash zone. The modelling of these phenomena was made possible by incorporating a moving shoreline boundary condition at the beach. As for regular waves, a good match for the shape of the wave profiles as well as phase-averaged quantities was obtained.

4.2. The roller breaking model

The roller model was initially suggested by Svendsen (1984) for a phase-averaged model. The basic concept is to divide the breaking wave into a region which is part of the irrotational wave motion and a roller region on top of this, in which a bulk of water is moved passively with the wave front towards the beach. This is sketched in Fig. 5. The vertical thickness of the roller region is denoted δ .

The introduction of the roller region leads to a discontinuity in the velocity profile for the horizontal velocity at the lower boundary of the roller region (see Fig. 5). Schäffer et al. (1993) re-derived the nonlinear shallow water equations for this modified velocity profile and added the classical dispersive Boussinesq terms. Madsen et al. (1997a) followed this approach, adding their enhanced dispersive Boussinesq terms. The resulting mass equation is identical to Eq. (2.1), while the momentum equation (Eq. (2.2)) was altered by the addition of a term $\partial R/\partial x$.

The quantity R is the vertically integrated excess momentum flux due to the roller and is a function of the roller thickness δ , the depth h , the volume flux P , the wave celerity c and the free surface elevation η :

$$R = \frac{\delta}{1 - \delta/d} (c - P/d)^2, \quad d = h + \eta. \quad (4.5)$$

In the time domain formulation, the roller thickness is determined by a heuristic geometrical approach. A critical slope of the wave front $\tan \phi$ is defined, and the toe of the roller is determined as the first point in which the surface slope exceeds this value. The roller region is then determined as the part of the wave profile lying above a line passing through the roller toe and having the critical slope $\tan \phi$. This is sketched in Fig. 6. To allow for

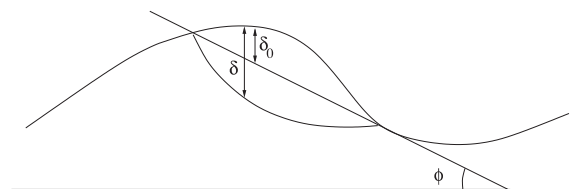


Fig. 6. Time domain roller detection. A roller thickness δ_0 is determined geometrically using a line of slope ϕ . Later on, δ_0 is multiplied by a constant factor f_δ to obtain the roller thickness δ .

a little more volume of the roller, the initial roller thickness is multiplied by a shape factor f_δ to obtain the roller thickness $\delta=f_\delta\delta_0$. Further, the limiting surface slope $\tan\phi$ is given a time dependence starting from $\tan\phi_B$ decaying to $\tan\phi_0$ within a time scale of $t_{1/2}$:

$$\tan\phi(t) = \tan\phi_0 + (\tan\phi_B - \tan\phi_0) \times \exp\left[-\ln 2(t - t_0)/t_{1/2}\right] \quad (4.6)$$

This is based on the observation that waves have rather steep fronts just before breaking, while they turn into a travelling bore state in the surf zone, with a much smaller limiting angle. For the Boussinesq model (Eqs. (2.1) and (2.2)), the parameter values $\phi_B=20^\circ$, $\phi_0=10^\circ$, $f_\delta=1.5$ and $t_{1/2}=T/5$ were selected by Schäffer et al. (1993) and Madsen et al. (1997a).

4.3. Adapting the roller model to the frequency domain

In the above approach, the roller thickness is determined as

$$\delta_0(x, t) = \eta(x, t) - \eta_{\text{toe}} - (x_{\text{toe}} - x)\tan\phi(t), \quad \delta_0 \geq 0 \quad (4.7)$$

when a spatial wave profile is given. Here subscript ‘toe’ refers to the toe of the surface roller. This expression is evaluated for fixed t . When the spatial variation of the wave field is only known for $x < x_0$, as is the case during the integration of a set of evolution equations, the latter term cannot be evaluated. This difficulty can be overcome by rewriting δ_0 in terms of a time series for η .

To allow for this, we assume that the roller region of the breaking wave travels with permanent form locally. That is $\delta_0 = \delta_0(x - ct)$ and thereby $\delta_{0,t} = -c\delta_{0,x}$ and similarly for η . Differentiating Eq. (4.7) with respect to x , and using the permanent form assumption locally yields $\delta_{0,t} = \eta_t - c \tan\phi(t)$, which is easily integrated to

$$\delta_0(x, t) = \eta(x, t) - \eta_{\text{toe}} - c \int_{t_{\text{toe}}}^t \tan\phi(t) dt, \quad \delta_0 \geq 0 \quad (4.8)$$

which can be evaluated for fixed x . This formulation is also feasible in time domain Boussinesq models, where it offers a significant simplification for the case of two horizontal dimensions (see Sørensen et al., 2004). When δ_0 is calculated using Eq. (4.8), the breaking criterion is changed to a critical value for η_t . Again, assuming that the wave travels with permanent form locally, we use $\eta_t > c \tan\phi$ as the breaking criterion. For c we use the estimate $c = v\sqrt{gh}$, where $v=1.3$ corresponds to the suggestion of Stive (1980). Note that using the linear phase speed for c is not appropriate, since this is known to be smaller than the phase speed of a breaking (and thus nonlinear) wave. Once δ_0 is determined, δ is found as $\delta=f_\delta\delta_0$ and R is calculated using Eq. (4.5).

In the wave equation (Eq. (2.3)), the inclusion of roller breaking results in the addition of the term R_{xx} at the right-hand side. Hence, following the derivation of Eq. (3.1), the roller effect can be included in the evolution equations as

$$a_{p,x} = -i \frac{\beta_{0,p}}{\beta_{1,p}} a_p - \beta_{s,p} \frac{h_x}{h} a_p + \frac{i}{\beta_{1,p}} \left[\hat{\mathcal{N}}_{p,xx} + \hat{\mathcal{R}}_{p,xx} \right] e^{i \int k_p dx}, \quad (4.9)$$

where $\hat{\mathcal{R}}_{p,xx}$ is the p th Fourier coefficient of R_{xx} , defined through $R_{xx} = \sum_{p=-\infty}^{\infty} \hat{\mathcal{R}}_{p,xx} e^{ip\omega t}$. Assuming that R , locally, is moving with constant form with the wave, i.e. $R=R(x-ct)$, we approximate R_{xx} by R_{tt}/c^2 . The time differentiation is performed after the Fourier transformation to the frequency domain, such that the breaking term at each frequency enters the model as

$$a_{p,x} = -i \frac{\beta_{0,p}}{\beta_{1,p}} a_p - \beta_{s,p} \frac{h_x}{h} a_p + \frac{i}{\beta_{1,p}} \left[\hat{\mathcal{N}}_{p,xx} - \frac{\omega_p^2}{c^2} \hat{\mathcal{R}}_p \right] e^{i \int k_p dx}, \quad (4.10)$$

where $\hat{\mathcal{R}}_p$ is defined similarly to $\hat{\mathcal{R}}_{p,xx}$.

4.4. Inclusion of mean water level variations in the model

The set of evolution equations (Eq. (4.10)) does not treat the mean flow variables $\bar{\eta}$ and \bar{P} . In all physical

situations of one-dimensional wave propagation, $\bar{P}_x=0$ due to mass flux conservation. Hence, there is no need to establish an equation for \bar{P} . For one-dimensional waves propagating towards a beach we have $\bar{P}=0$. The mean water elevation $\bar{\eta}$, however, is nonzero.

We can obtain such an equation by time averaging the momentum equation (Eq. (2.2)). In this averaging, we use that the time average of a time derivative of a flow variable is zero for a periodic flow. We further assume that $\bar{\eta}$ is of similar magnitude as the bound second-order waves and is slowly varying in space. This allows for calculating $\bar{\eta}$ with basis in the free first-order wave field and to neglect derivatives of higher order than the first derivative of $\bar{\eta}$. With these considerations, we get from Eq. (2.2) with the added roller term:

$$\bar{\eta}_x = -\frac{1}{gh} \left\langle \frac{P^2}{h} + \frac{1}{2} g \eta^2 + R \right\rangle_x \quad (4.11)$$

where the brackets $\langle \rangle$ denote time averaging similarly to the over-bar. A similar equation was derived by Madsen et al. (1997a).

The above equation can be integrated numerically along with the integration of the evolution equations. The nonlinear time series within the averaging bracket is calculated from the wave amplitudes with the aid of inverse FFTs in each step. The mean value of R is easily provided as part of the breaking calculation. The spatial derivative involved can be calculated numerically, using a backward finite difference approximation. Writing Eq. (4.11) as $\bar{\eta}_x = -\bar{A}_x / gh$, this can be done with fourth-order accuracy by fitting a polynomial through the actual point (x, \bar{A}) plus the last four points and evaluating the polynomials first derivative in the actual point. However, we found this approach nonfeasible, due to a lack of smoothness of \bar{R} . As a more robust alternative, the first-order derivative was therefore obtained by fitting a line through the actual point (x, \bar{A}) plus the last four points and using the slope of this line as the derivative of \bar{A} . A comparison between the two approaches for calculation of $\bar{\eta}$ for the regular wave test of Section 5 gave graphically identical results, but the latter approach could be used with larger spatial integration steps.

4.5. How the setup affects the wave field

In the above derivation, we have formally assumed that $\bar{\eta}$ is of the same order of magnitude as the second-order bound waves. We can therefore consistently calculate the harmonic wave field without taking the setup into account. However, within the breaking zone, practical experience show that the setup can be of similar magnitude as the harmonic amplitudes, and therefore it may be reasonable to include the effect of the setup into the calculations of the wave field.

The summation ranges of the nonlinear interaction terms in Eq. (2.8) allows for inclusion of a setup through the zeroth harmonic. The interaction coefficient, however, must be modified slightly when one of the interacting frequencies is zero. We consider the nonlinear term

$$N_p = -\frac{ig}{\beta_{1,p}} \sum_{s=p-N}^N (k_s + k_{p-s})^2 \times \left(\frac{1}{2} + \frac{1}{gh} \frac{\omega_s}{k_s} \frac{\omega_{p-s}}{k_{p-s}} a_s a_{p-s} \right) e^{-i \int (k_s + k_{p-s} - k_p) dx}, \quad (4.12)$$

see Eq. (2.8). For $s=0$ we get

$$N_p \text{ term from } s=0 = -\frac{ig}{\beta_{1,p}} k_{p-s}^2 \left(\frac{1}{2} + 0 \right) a_0 a_p = -\frac{ig}{\beta_{1,p}} k_p^2 \frac{1}{2} \bar{\eta} a_p, \quad (4.13)$$

where the zero in the interaction coefficient arises because $\bar{P}=0$. With this modification of the coefficient, and a similar modification of the coefficient for $p-s=0$, the influence of the setup can be treated through the nonlinear terms. The above approach has been used for all frequency domain results for breaking waves in this paper.

5. Results for regular waves

We here present results for breaking of regular waves. The physical test chosen is the test of Ting and Kirby (1994) for spilling breakers. In these experiments, waves with a period of 2 s propagate over a uniformly sloping beach of slope 1:35. The initial

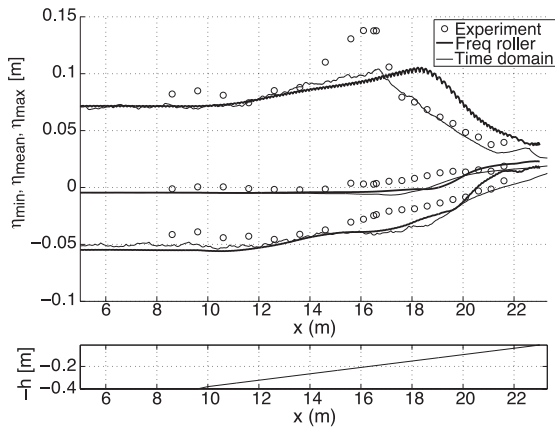


Fig. 7. Envelope for the spilling breaker test of Ting and Kirby (1994). Frequency domain roller model with default parameters, time domain model and experimental results. The lower panel shows the bathymetry.

depth is 0.4 m and the initial wave height 0.125 m. To simulate this test with the time domain model, a grid spacing of 0.02 m and a time step of 0.005 s were used. Within the breaking model, the parameters $\phi_B=20^\circ$, $\phi_0=10^\circ$, $T_{1/2}=T/5$ and $f_\delta=1.5$ were chosen, as recommended by Madsen et al. (1997a).

As a first attempt, the frequency domain model was run with the same parameters and with $c = 1.3\sqrt{gh}$.

Seven harmonics were included in the calculations, and the roller term was calculated with a resolution of 128 points in the time series.

Fig. 7 shows the wave envelope for the time domain and frequency domain simulations. Also, the experimental values are plotted. The time domain model does not reach the experimentally observed wave height at the initiation of breaking. This is due to the assumption of weak nonlinearity in this model, and has been commented on by Madsen et al. (1997a) as well. Second, the initial trough level and mean water level are smaller than for the experimental results, leading to an overall lowering of the wave profile of the numerical solution. The breaking point and the decay of the crest elevation, however, are modelled satisfactorily.

For the frequency domain model, the wave shoals a little less than the time domain solution. The breaking initiates later than for the time domain model. This results in a rather poor comparison with the results of the time domain model and the experimental results.

The frequency domain model can be tuned to match the results of the time domain model by adjusting the breaking parameters. Thus for $\phi_B=16^\circ$, $\phi_0=8^\circ$, $T_{1/2}=T/5$, $f_\delta=1.5$ and $c = 1.1\sqrt{gh}$, the envelope of the wave field is plotted in Fig. 8 along with

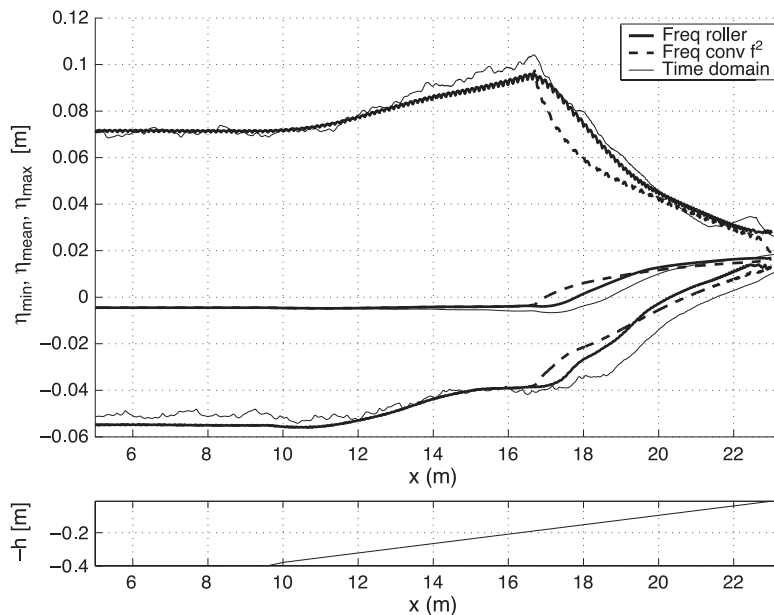


Fig. 8. Wave envelopes for f^2 -weighted conventional breaking, roller breaking and time domain model. The lower panel shows the bathymetry.

the time domain results as well as results for the Battjes and Janssen (1978) breaking model with f^2 -weighted dissipation. With the adjusted parameters, the point of initial wave breaking and the decay of the crest height match the time domain results well. The mean water level and the trough level are both increasing inside the surf zone, with a similar shape as the time domain results, although the initial growth is 1–2 m ahead of the time domain results.

While the adjustment of the breaking parameters leads to a better match with the time domain results, it is unsatisfying that the values of the parameters now differ between time domain and frequency domain. However, examining the model performance for a set of ‘best match’ parameters’ is the first step in investigating the overall quality of the model. A second step would then be to establish a general set of recommended parameters through application of the model to several test cases. For the present study, however, we regard the first step as sufficient.

The f^2 -weighted breaking results were obtained using seven harmonics and the parameters $\alpha=1.2$ and $\gamma=0.8$. For this test of regular waves, H_{rms} was replaced by $H_{\text{reg}} = 4 \sum_{p=1, \text{podd}}^N |a_p|$, being the wave height of a

perfectly regular wave. Further, the breaking scheme was not activated until $x=16.7$ m, since otherwise breaking would initiate much earlier on the slope. When calculating the mean water variation, the formula (4.11) was used, omitting the \bar{R}_x term, since this is not generally known for this breaking formulation. The crest height within the surf zone of this formulation decays rapidly in the first part of the surf zone, leading to smaller wave heights than for the other models. The growth of crest height and mean water level initiates about 1 m before the results of the roller breaking formulation of the frequency domain, expectedly due to the omission of the \bar{R}_x term.

Spatial profiles of the waves are compared in Fig. 9 for the time domain model and the frequency domain roller model. The plot is stacked in time and the vertical scaling of the waves is arbitrary. Up till the point of breaking, the wave shape is rather similar between the models, while as the waves transform through the surf zone, the frequency domain results show a lack of steepening and asymmetry, when compared to the time domain results. The waves of the frequency domain model do not lean forward to the same extent as the waves of the time domain

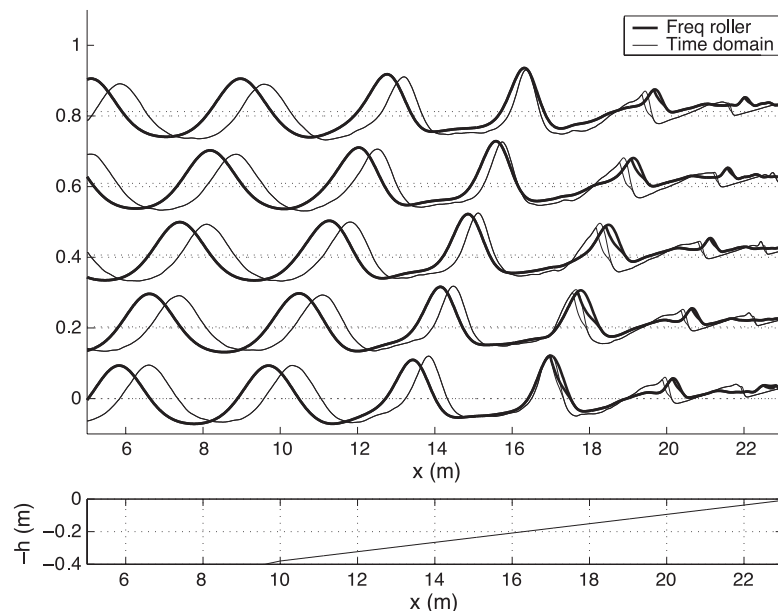


Fig. 9. Profiles in space for frequency domain roller model with adjusted parameters. Comparison with time domain model. The profiles are plotted for fixed time values. The vertical position of the mean water level has been shifted vertically by t/T (time relatively to wave period). This time measure is shown on the vertical axis. The lower panel shows the bathymetry.

model, and the characteristic sawtooth shape of the time domain waves is not achieved. Further, the waves within the frequency domain model clearly propagate with a larger phase speed than the waves of the time domain model. We return to this aspect in Section 7.

Another way to assess the shape of the waves is to consider time series at different locations, as depicted in Fig. 10. Time series of the free surface elevation from the frequency domain roller model are compared to time domain results and laboratory data. To ease the comparison, the profiles have been aligned horizontally, such that all crests occur at $t=1$ s. The time domain data show a smaller crest elevation than for the measured data, as well as a lack of steepness in $x=16.77$ m. This has already been discussed in relation to Figs. 8 and 9. As the wave enters the surf zone, the comparison becomes progressively better, and from $x=17.98$ m and onwards, a satisfactory description of the wave shape is achieved—including the characteristic sawtooth shape of the breaking waves.

For $x=16.77$ m, just after initiation of breaking, the profiles of the frequency domain roller model match the time domain results rather well, the slightly smaller wave height of the frequency domain results being the largest deviation. Inside the breaking zone, the waves of the frequency domain roller model tend not to lean as much forward as for the time domain model and measured data. Also, while the data and time domain model results maintain a straight ‘back’ to the right of the crest, the frequency domain roller results show a more humped look.

In Fig. 11, results from the time domain model, the frequency domain roller model and the f^2 -weighted conventional breaking model are shown for six locations equidistantly spaced between $x=16.7$ m and $x=21$ m. The results obtained with f^2 -weighted breaking clearly show a smaller wave height for $x=17.56$ m and $x=18.42$ m when compared to the results of the frequency domain roller model. For these smaller waves, the back of the wave is more straight than for the roller model. For the three last frames $x=(19.28, 20.14, 21.0)$ m, however, the time

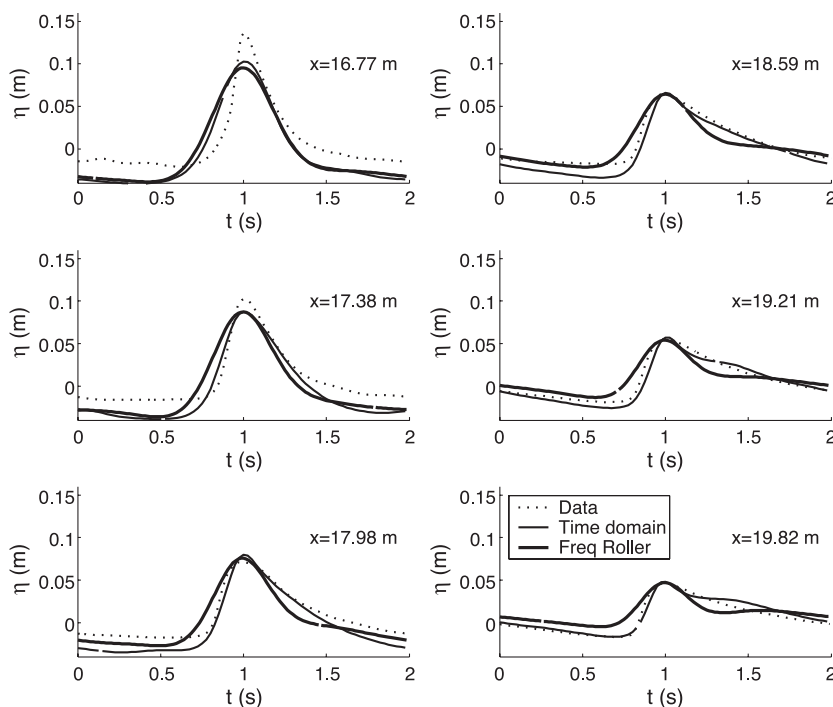


Fig. 10. Time series for measured data, time domain model and frequency domain roller model. The time series are aligned horizontally, so the crest is always at $t=1$ s.

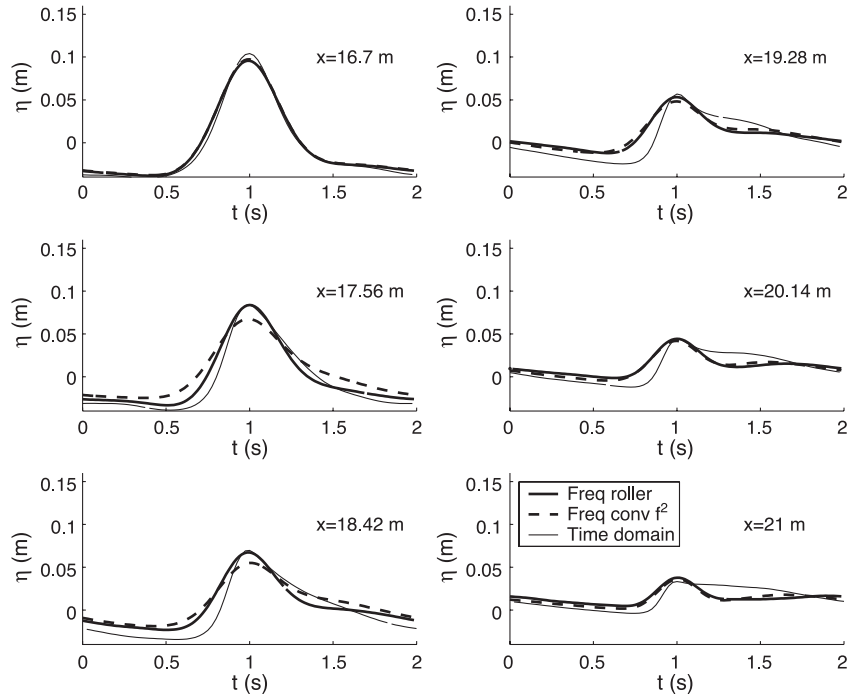


Fig. 11. Time series for f^2 -weighted conventional breaking, roller breaking and time domain model. The time series are aligned horizontally, so the crest is always at $t=1$ s.

series are very similar to the time series of the frequency domain roller model. This includes the hump at the back of the roller in $x=19.28$ m and $x=20.14$ m. In the last two frames, the time series of the frequency results are almost symmetric, in contrast to the asymmetric shape of the time domain results.

This specific test of regular waves thus suggests that a conventional breaking model with f^2 -weighted breaking is able to produce wave profiles of a similar quality as the frequency domain roller model.

6. Results for irregular waves

We now show the results for a test of irregular waves. A faithful description of irregular waves requires that the breaking model is able to detect when a given wave in a wave series is breaking, while nonbreaking waves should be left unaltered. As the frequency domain roller breaking model is

based on a processing of the actual deterministic time series for the local wave field, it can be expected that the model is able to localise the effect of breaking better than a conventional bulk breaking model.

To test this hypothesis, we choose the test of [Beji and Battjes \(1993\)](#) for irregular waves breaking over a submerged bar. The bar topography is identical to the one in [Fig. 1](#). The specific test chosen is for a narrow-banded spectrum of peak frequency $f_{\text{peak}}=0.4$ Hz and a significant wave height of 4.2 cm. The wave field was sampled at 10 Hz in six stations, as shown in [Fig. 1](#). The length of the sampled time series is $T_{\text{dur}}=899.68$ s, corresponding to a frequency resolution of $f_1=1/T_{\text{dur}}=1.11\times 10^{-3}$ Hz. For the frequency domain simulations, the maximum frequency was chosen as $f_{\text{max}}=2.0$ Hz, giving a maximum error in linear phase speed of 23% at the largest depth of 0.4 m. This is a rather large error, and would usually lead to the choice of a smaller cutoff frequency for the spectrum. However, when inspecting time series for the free surface elevation

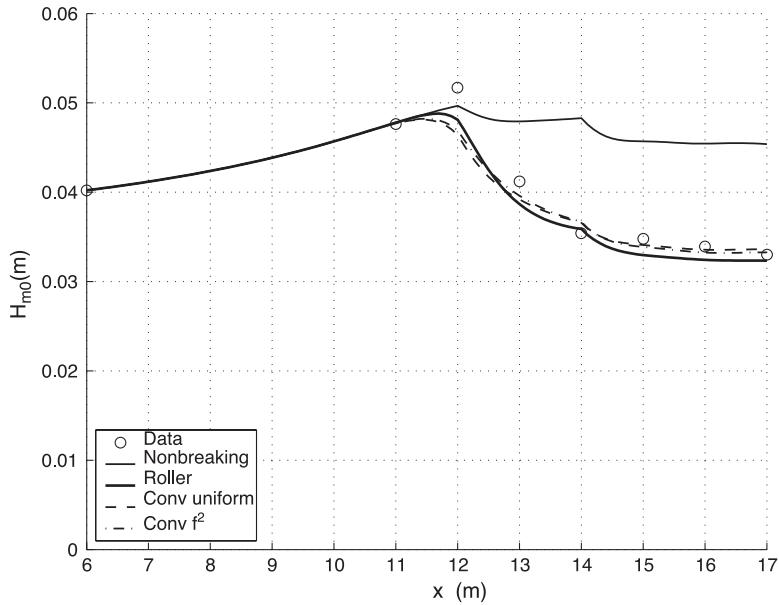


Fig. 12. Significant wave height, H_{m0} for the experimental data, a model run without breaking, the roller model, uniform breaking and f^2 -weighted breaking. The abscissa, x , is the spatial coordinate along the direction of wave propagation.

at the top of the bar, it was found that a smaller cutoff frequency lead to a poor representation of the wave profiles, with spurious wiggles at the cutoff frequency. At the bar top, the error in linear phase speed is only 0.4% for $f=2$ Hz. We have therefore chosen to retain this relatively high cutoff frequency. This leads to a total number of 1800 frequencies. The number of points in the time series used for

calculation of the nonlinear term and the breaking term was chosen to be 8192. The parameters $\phi_B=11^\circ$, $\phi_0=5^\circ$, $T_{1/2}=T_{\text{peak}}/10$, $f_\delta=1.5$ and $c=1.1\sqrt{gh}$, were used for the roller calculations. These parameters were chosen to fit the wave height decay of the experimental results. Admittedly, one set of standard parameters for the frequency domain roller breaking model would be preferable. How-

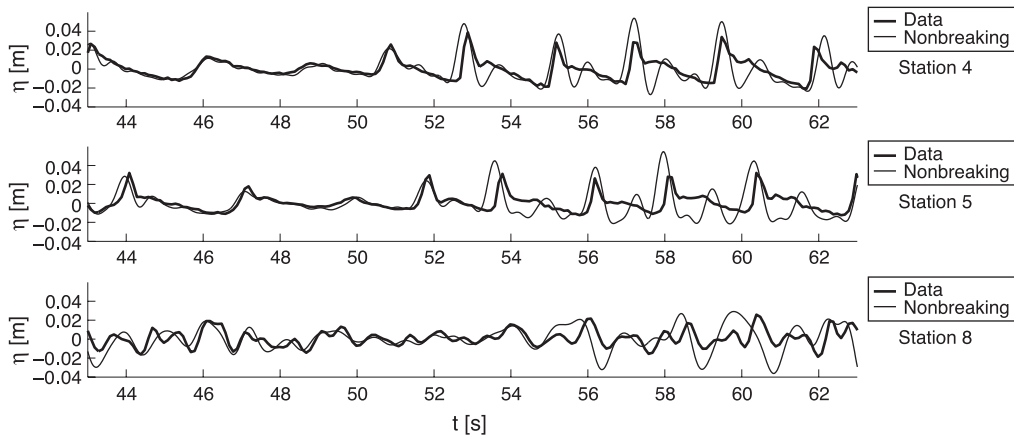


Fig. 13. Surface elevation of data and nonbreaking model.

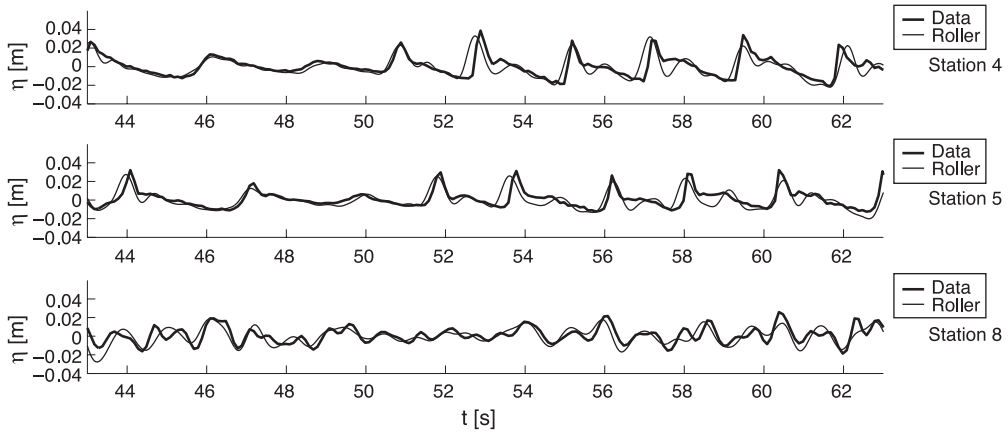


Fig. 14. Surface elevation of data and roller breaking model.

ever, as a first start, it is convenient to study how the model performs for a set of parameters fitting the wave height decay well.

Simulations were also carried out with the conventional breaking model, for uniform as well as f^2 -weighted dissipation. Here the parameters $\alpha=1.0$, $\gamma=0.6$ were used for the uniformly weighted case, and $\alpha=1.2$, $\gamma=0.65$ for the f^2 -weighted case.

In Fig. 12, H_{m0} is shown for the experimental data, a model run without breaking, the frequency domain roller model, uniform conventional breaking and f^2 -weighted conventional breaking. H_{m0} is an estimate of the significant wave height H_s , and is defined by $H_{m0}=(16m_0)^{1/2}$, where m_0 is the zeroth moment of

the spectral energy content. For a discrete spectrum we determine this as

$$m_0 = \sum_{p=-N}^N |\eta_p|^2. \tag{6.1}$$

The breaking process leads to a substantial decay in H_{m0} as the waves pass the bar. All the breaking models are calibrated satisfactorily to match the experimental points.

We now examine the shape of the wave profiles. We focus on a group of breaking waves, preceded by a few waves of smaller amplitude. In Fig. 13, time series of the experimental data and the nonbreaking

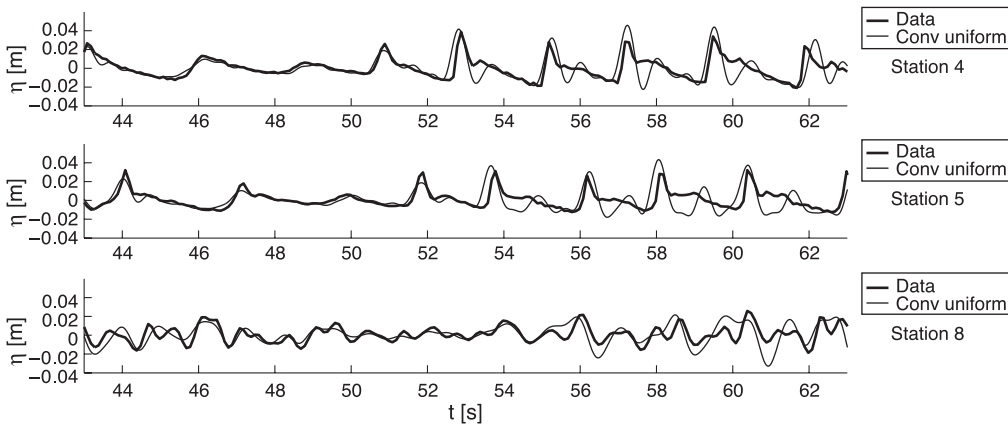


Fig. 15. Surface elevation of data and conventional breaking model with uniformly weighted breaking.

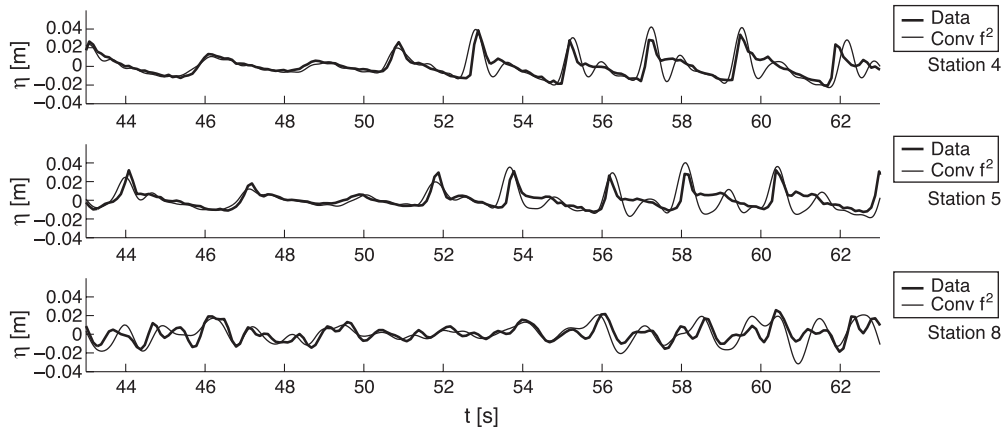


Fig. 16. Surface elevation of data and f^2 -weighted conventional breaking model.

model are plotted for stations 4, 5 and 8, corresponding to the midpoint of the bar top, the upper down-wave corner of the bar and the lower down-wave corner of the bar. For the nonbreaking waves, the model matches the experimental data with only small discrepancies, while for the breaking waves, the simulated waves are too high, and secondary crests are formed, following the primary waves. In the last station, the comparison between the model and experiments is rather poor.

The results of the roller breaking model and the conventional breaking model with uniform breaking are shown in Figs. 14 and 15, respectively. For the breaking waves in stations 4 and 5, both of the

breaking models produce secondary wiggles following the primary waves. This tendency, however, is not as strong for the roller model, as for the conventional breaking model. In station 5, the sawtooth shape of the breaking waves is completely lost by the conventional model, while the roller model retains some asymmetry for the profiles.

Results for f^2 -weighted conventional breaking are shown in Fig. 16. The results are qualitatively similar to the results obtained with uniform weighting of the dissipation. A direct comparison of the two sets of results of conventional breaking shows that the f^2 -weighting reduces the depth of the spurious wave trough following the crests of the breaking waves

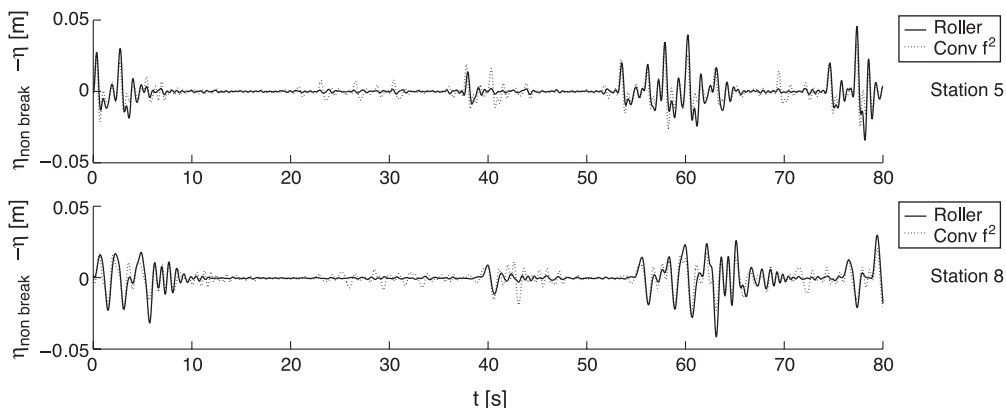


Fig. 17. Surface elevation of the nonbreaking simulation minus the surface elevation for a simulation including wave breaking. The solid line is results of the roller breaking model while the dotted line is results of f^2 -weighted breaking.

slightly. Also the asymmetry is slightly improved, although none of the simulations here presented are able to reproduce the sawtooth shape of the experimental wave profiles.

Having examined the shape of the breaking waves, we now return to the ability of the breaking models of localising the actual breaking events. This is examined in Fig. 17, which shows $\eta_{\text{nonbreak}} - \eta$ for the simulations carried out with the roller model and the f^2 -weighted conventional breaking model, respectively. Here η_{nonbreak} is simply the results of a simulation with the wave breaking turned off. The time series depicted cover the first 80 s of the experimental time series. For waves that have not been breaking, $\eta_{\text{nonbreak}} - \eta$ is zero, while wave crests that have been breaking are characterised by nonzero values. For the roller model, the broken wave crests are easily identified, and $\eta_{\text{nonbreak}} - \eta$ is clearly zero between these crests. Remarkably, the same holds for the results of the f^2 -weighted breaking model, except for an event of spurious breaking around $t=28$ s. Thus, although the conventional breaking model does not operate on the time series, but rather on the spectrum, the effect of breaking is well localised to the actual broken wave crests in the time series. The results for the uniformly weighted breaking model are similar with respect to the ability of localising the breaking wave crests, and are therefore not shown here.

For this test of irregular waves, we conclude that the wave profiles obtained with the roller breaking model are more asymmetric than for the bulk dissipation models. However, as all the simulated results have problems with secondary crests in the profiles of breaking waves, we do not regard the improvement obtained with the roller breaking model as substantial. Further, and rather surprising, we observe that the bulk dissipation model is able to localise the breaking wave crests satisfactorily.

7. Analysis of the embedded amplitude dispersion of the models

As was seen in Fig. 9, the waves calculated with the frequency domain model travel faster than the corresponding waves of the time domain model. This observation is valid both before and after breaking, and the deviation in phase speeds is therefore

expected to relate to properties of the two models in their nonbreaking formulations. As the two models have identical linear dispersion properties, the difference in phase speed must be due to a difference in the description of amplitude dispersion in the models.

We thus here analyse the amplitude dispersion in the models using a third-order Stokes type perturbation analysis.

7.1. Analysis of time domain models

Madsen and Sørensen (1993) carried out such an analysis for the time domain model (Eq. (2.3)) in its strictly quadratic formulation, i.e. under the approximation (I) (see Section 2.1). We here extend the analysis to include the full nonlinear term. Thus for constant depth, we substitute the following solution ansatz into the time domain model (Eq. (2.3))

$$\eta(x, t) = \frac{\varepsilon}{k_1} \cos\theta + \frac{\varepsilon^2}{k_1} \tilde{A}_2 \cos 2\theta + \frac{\varepsilon^3}{k_1} \tilde{A}_3 \cos 3\theta \quad (7.1)$$

with

$$\theta = \omega t - k_1 x \quad \omega = \omega_1 (1 + \varepsilon^2 \omega_{13}) \quad (7.2)$$

and where $\varepsilon = k_1 A_1$ is assumed small. This solution constitutes a primary wave with bound harmonics at second and third order, with a modulated angular frequency, ω . The coefficients (\tilde{A}_2 , \tilde{A}_3 , ω_{13}) are dimensionless functions of kh , being of order $O(1)$ in the ε -hierarchy.

Insertion of this ansatz leads to a hierarchy of equations in different orders of ε . At first order, the linear dispersion relation of the model is recovered, while at second order, an explicit expression for \tilde{A}_2 is found. At third order, solutions for \tilde{A}_3 and ω_{13} are obtained. The solution for ω_{13} is

$$\omega_{13} = \frac{9}{16} \frac{1}{\kappa^4} \times \frac{1 + 2(B + 1/9 - \Gamma/3)\kappa^2 + \left(B^2 + \frac{2}{9}B - \frac{2}{3}\Gamma B\right)\kappa^4}{1 + (2B + 1/3)\kappa^2 + B(B + 1/3)\kappa^4} \quad (7.3)$$

with $\kappa = kh$. In the analysis, the last nonlinear term in Eq. (2.3) has been written as $[P^2/(h + \Gamma\eta)]_{xx}$, and Γ is

therefore a Boolean variable, toggling between the full nonlinear term ($\Gamma=1$) and the simplified quadratic formulation, as implied by approximation (I) ($\Gamma=0$). For $\Gamma=0$, the result of Madsen and Sørensen (1993) is recovered, although the coefficients of the κ^4 terms were not given explicitly in their paper.

7.2. Analysis of frequency domain models

In the frequency domain model, ω_p are fixed numbers and are therefore not allowed to be modulated. The modulation of the wave speed therefore enters through a modulation of the wave number, and we thus search for a solution of the form (7.1) but with

$$\theta = \omega_1 t - kx \quad k = k_1(1 - \varepsilon^2 k_{13}). \tag{7.4}$$

Matching this solution ansatz (Eq. (7.1)) with the expansion (Eq. (2.4)) gives

$$a_1 = \frac{1}{2} \frac{\varepsilon}{k} e^{-i(k-k_1)x} \tag{7.5a}$$

$$a_2 = \frac{1}{2} \frac{\varepsilon^2}{k} \tilde{A}_2 e^{-i(2k-k_2)x} \tag{7.5b}$$

$$a_3 = \frac{1}{2} \frac{\varepsilon^3}{k} \tilde{A}_3 e^{-i(3k-k_3)x}. \tag{7.5c}$$

We write the evolution equations in the short form

$$a_{p,x} = i \sum_{s=p-N}^N W_{s,p-s} a_s a_{p-s} e^{-i(k_s+k_{p-s}-k_p)x} \tag{7.6}$$

where the interaction coefficient $W_{s,p-s}$ is defined by the identity of the above equation with Eq. (2.8) for constant depth. In the presence of only three harmonics, the evolution equations can then be written

$$a_{1,x} = 2iW_{2,-1}a_2a_{-1}e^{-i(k_2-2k_1)x} \tag{7.7}$$

$$a_{2,x} = iW_{1,1}a_1^2e^{-i(2k_1-k_2)x} \tag{7.8}$$

$$a_{3,x} = 2iW_{2,1}a_1a_2e^{-i(k_1+k_2-k_3)x}. \tag{7.9}$$

Insertion of Eqs. (7.5a)–(7.5c) now gives a hierarchy of equations in ε . The (ε^0 , ε^1) equations are identically satisfied, while at $O(\varepsilon^2)$, Eq. (7.8) yields the solution for \tilde{A}_2 . At $O(\varepsilon^3)$, Eq. (7.7) gives the solution for k_{13} ,

while Eq. (7.9) gives the solution for \tilde{A}_3 . The solutions are

$$\begin{aligned} k_{13} &= \frac{W_{2,-1}W_{1,1}}{2k_1^3(k_2 - 2k_1)}; \\ \tilde{A}_2 &= \frac{W_{1,1}}{2k_1(k_2 - 2k_1)}; \\ \tilde{A}_3 &= \frac{W_{2,1}W_{1,1}}{2k_1^2(k_2 - 2k_1)(k_3 - 3k_1)}. \end{aligned} \tag{7.10}$$

To relate k_{13} to ω_{13} , we consider the sketch in Fig. 18. Here a curve representing the linear dispersion relation of the model is drawn. Corresponding pairs of (ω, k) for linear waves, produce points on the curve, while nonlinear waves produce points above the linear dispersion curve, since their phase speed ω/k is larger than for linear waves. Such a nonlinear wave is represented in the figure by point (C). If this nonlinear wave is described using a modulation of ω , it originates from the linear wave (A), sharing its wave number k_1 . The vertical distance between (A) and (C) is $\varepsilon^2\omega_1\omega_{13}$. Similarly, if the nonlinear wave is described using a modulation of the wave number, it originates from the linear wave (B) having the same angular frequency (ω_1) and the horizontal distance between this wave and the nonlinear wave is $\varepsilon^2k_1k_{13}$. We can relate k_{13} to ω_{13} by considering the triangle defined by these two linear waves and the nonlinear wave. As the

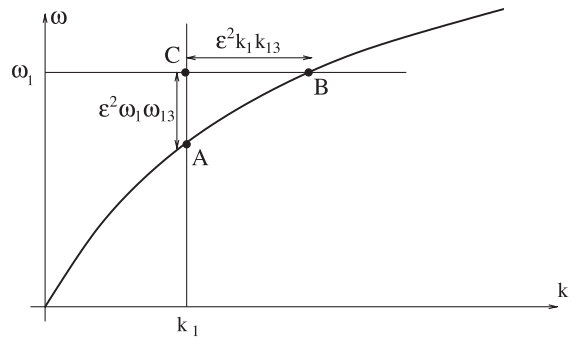


Fig. 18. Dispersion diagram. Two linear waves (A, B) on the linear dispersion curve and a nonlinear wave (C). The nonlinear wave can be described by modulation of ω for wave (A) or modulation of k for wave (B).

slope of the dispersion curve is $\partial\omega/\partial k$ we have $\varepsilon^2\omega_1\omega_{13}=\varepsilon^2k_1k_{13}(\partial\omega/\partial k)$, and thereby

$$\omega_{13} = \frac{c_g}{c_{lin}} k_{13}. \tag{7.11}$$

Note that since the deviation between the wave numbers and angular frequencies for the linear and nonlinear waves are of order $O(\varepsilon^2)$, c_g , the group velocity, and c_{lin} , the linear phase speed, can be evaluated in any of the three points as desired.

With these results, we can compare the description of amplitude dispersion in the two models by comparing the values of ω_{13} as function of frequency. This is done in Fig. 19, where the values have been normalised by the value of ω_{13} for regular Stokes waves, which is taken as the target solution. For the Stokes waves, the solution for a zero mass flux is used, corresponding to wave propagation towards a beach. This solution is given in Fenton (1985) and reads in our notation

$$\omega_{13} = \frac{2 + 7S^2}{4(1 - S)^2} - \frac{1}{2} \frac{1}{\kappa \tanh \kappa}, \quad S = \operatorname{sech} 2\kappa \tag{7.12}$$

where the last term ensures a zero mass flux in the direction of wave propagation. If the last term is

omitted, the solution corresponding to a zero Eulerian mean velocity below wave trough level is recovered. The ratio between these two solutions for ω_{13} can be as large as 2.5, and it is therefore important to specify which reference solution is used for normalising.

From Fig. 19, the time domain model’s description of amplitude dispersion agrees well with the target solution until, say, $\omega\sqrt{h/g} = 0.5$, where it decays towards zero. Actually, for $\omega\sqrt{h/g} = 1.3$ a negative value of ω_{13} is achieved. This is unphysical and is due to the violation of the long wave assumption of the model derivation for large frequencies. Note that these results differ from those of Madsen and Sørensen (1993) with respect to two points: first, we here analyse the full nonlinear term and second, we use the Stokes reference solution with a zero mass flux.

The evolution equations show a strong over-prediction of the amplitude dispersion, being as large as twice the value of the Stokes solution for $\omega\sqrt{h/g} \approx 0.75$. For the test of Ting and Kirby (1994), $\omega\sqrt{h/g} = 0.6$ for the flat section of the bathymetry. Here ω_{13} of the evolution equations is

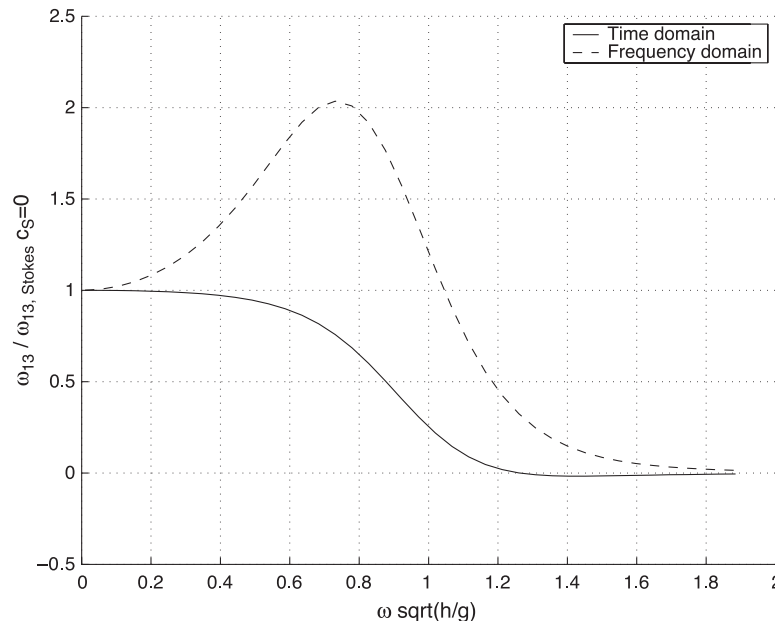


Fig. 19. ω_{13} for the time domain model (Eq. (2.3)) and the frequency domain model (Eq. (2.8)) normalised by the result for Stokes waves for a zero mass flux.

more than twice as large as for the time domain model, and the plot therefore explains the deviations in phase speeds observed. For larger values of $\omega\sqrt{h/g}$, ω_{13} decays towards zero for the evolution equations.

The difference in the description of amplitude dispersion is due to the approximations applied, when deriving the evolution equations. For the special case of a primary wave with bound higher harmonics, it is possible to avoid these approximations, since the solution for the wave field is known a priori. We can therefore derive evolution equations with different combinations of these approximations for this special case. Under approximation (I), Eq. (2.5) can be written

$$\begin{aligned}
 & [\beta_{4,p} \partial_x^3 - i\beta_{3,p} \partial_x^2 - \beta_{2,p} \partial_x + i\beta_{1,p}] \partial_x a_p \\
 &= -g \sum_{s=p-N}^N \left[\left(\frac{1}{2} a_s a_{p-s} + b_s b_{p-s} \right) e^{-i(k_s+k_{p-s})x} \right]_{xx} \\
 & \times e^{ik_p x}. \tag{7.13}
 \end{aligned}$$

We are looking for a bound wave solution of the form

$$\begin{aligned}
 \eta(x,t) &= \sum_{p=-N}^N \tilde{a}_p e^{i(\omega_p t - \tilde{k}_p x)} \\
 P(x,t) &= \sum_{p=-N}^N \tilde{b}_p e^{i(\omega_p t - \tilde{k}_p x)}, \tag{7.14}
 \end{aligned}$$

with $(\tilde{a}_p, \tilde{b}_p)$ being real constants and $(\omega_p, \tilde{k}_p) = p(\omega_1, \tilde{k}_1)$, where \tilde{k}_1 is the nonlinear wave number of the first harmonic. Matching these expansions with Eq. (2.4) gives

$$a_p(x) = \tilde{a}_p e^{-i(\tilde{k}_p - k_p)x} \quad b_p(x) = \tilde{b}_p e^{i(\tilde{k}_p - k_p)x} \tag{7.15}$$

and therefore $\partial_x a_p = -i(\tilde{k}_p - k_p)a_p$. This allows us to express the differential operator at the left-hand side of Eq. (7.13) as a scalar. Similarly, without any approximation, the double differentiation at the right-

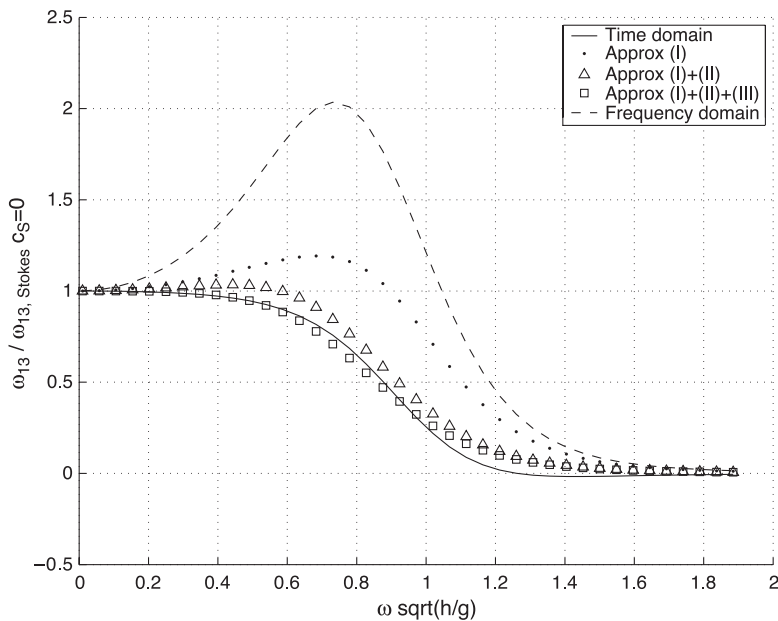


Fig. 20. ω_{13} for successive application of approximation (I) through (VI).

hand side, can be replaced by a multiplication with $-(k_s+k_{p-s})^2$. Finally, substitution of Eq. (7.15) into Eq. (2.1) gives $\tilde{b}_p=\tilde{a}_p\omega_p/k_p$, also free of approximations. With these modifications, we rewrite Eq. (7.13) to the form of Eq. (7.6) with

$$W_{s,p-s} = -g \frac{(k_s^{IV} + k_{p-s}^{IV})^2 \left(\frac{1}{2} + \frac{1}{gh} \frac{\omega_s}{k_s^{III}} \frac{\omega_{p-s}}{k_{p-s}^{III}} \right)}{\beta_{4,p}(k_p^{II} - k_p)^3 + \beta_{3,p}(k_p^{II} - k_p)^2 + \beta_{2,p}(k_p^{II} - k_p) + \beta_{1,p}}. \quad (7.16)$$

The new wave numbers introduced have the following purpose: $k_j^{II}=(k_j, \tilde{k}_j)$ corresponds to approximation (II) (on,off), respectively. Similarly $k_j^{III}=(k_j, \tilde{k}_j)$ toggles approximation (III) (on,off) and $k_j^{IV}=(k_j, \tilde{k}_j)$ toggles approximation (IV) (on,off). The approximations are listed in Section 2.1. Thus by inserting different combinations of free and bound wave numbers into the kernel (Eq. (7.16)), the influence of the different approximations can be analysed.

In Fig. 20, five curves are drawn, corresponding to no approximations (the time domain model), approximation (I), approximation (I)+(II), approximation (I)+(II)+(III) and evolution equations, i.e. approximations (I)+(II)+(III)+(IV). The results show that approximation (I) (neglect of η in the denominator of the nonlinear term) increases the amplitude dispersion, while approximation (II) (truncation of the linear operator) and (III) (linear flux approximation in the nonlinear term) decreases the amplitude dispersion. The large amplitude dispersion of the evolution equations is caused by approximation (IV) (neglect of derivatives of a_p in nonlinear terms) which is seen to affect the amplitude dispersion far more strongly than any of the other approximations.

8. Conclusions

In this paper, the possibility of transferring methods from time domain Boussinesq models to their frequency domain counterparts has been exploited. We have investigated how well results of the frequency domain Boussinesq models match results of the corresponding time domain models. Three aspects have been addressed, using the evolution equations of Madsen and Sørensen (1993) as example throughout. First, we have demonstrated that

the computational efficiency of evolution equations can be significantly improved, by calculating the nonlinear terms by the aid of Fast Fourier Transforms. For N frequencies, the computational effort is thus reduced from $O(N^2)$ to $O(N \log N)$. A practical example has shown that evolution equations provide a fast alternative to time domain Boussinesq models, since for the specific irregular wave test chosen, the evolution equations could be solved 100 times faster than the corresponding time domain formulation.

Second, as an attempt to improve the traditional wave breaking formulations, the surface roller breaking model, known from time domain Boussinesq formulations has been adapted into the framework of evolution equations. An equation for the variation of the mean water level has been derived as well and incorporated into the model. Even though the new breaking model is based on direct processing of time series for the surface elevation in each spatial point, the quality of the resulting wave profiles has been found not to improve the results of an f^2 -weighted conventional breaking model significantly. The new breaking model can therefore not be recommended in its present form, as conventional breaking models are much simpler, yet giving results of similar quality.

Third, motivated by comparisons of results of the evolution equations of Madsen and Sørensen (1993) and the corresponding time domain formulation, the embedded amplitude dispersion of these wave models has been analysed. For the time domain formulation, the effect of the ‘full’ (not only quadratic) nonlinear term has been analysed for the first time. It has been found that the embedded amplitude dispersion in the evolution equations of Madsen and Sørensen (1993) can be more than twice as large as the reference solution of Stokes waves on a zero mass flux and more than three times larger than for the corresponding time domain model. Further analysis has shown that this difference between the models is mainly due to the neglect of spatial derivatives of the wave amplitudes in the nonlinear terms of the evolution equations.

These results show that the evolution equations of Madsen and Sørensen (1993) are less accurate than the corresponding time domain model. While the Fourier series representation is ideal for describing a spectrum of linear waves, the representation of coherent bound waves—as nonlinear breaking waves is an example of—is not as accurate. This is in line with the practical

violation of the assumption of weak nonlinearity, applied when deriving the model and could be the reason why the roller model does not improve the wave profiles when compared to the results of conventional breaking models. In conclusion, the main justification for evolution equations is thus their computational efficiency, which makes it possible to treat a large number of frequencies (corresponding to a long time series) much more efficiently than for time domain models. This may be of interest for two horizontal dimensions, where the spatial and temporal resolution for time domain models is still limited by computational resources.

Acknowledgements

This work was financially supported by the Danish Technical Research Council (STVF grant no. 9801635). This support is greatly appreciated.

References

- Abbott, M.B., Larsen, J., Madsen, P.A., Tao, J., 1983. Simulation of wave breaking and runup. Seminar on Hydrodynamics of Waves in Coastal Areas, 20th Congr. of IAHR. IAHR, Moscow.
- Agnon, Y., Sheremet, A., 1997. Stochastic nonlinear shoaling of directional spectra. *J. Fluid Mech.* 345, 79–99.
- Battjes, J.A., Janssen, J.P.F.M., 1978. Energy loss and set-up due to breaking in random waves. Proceedings of the 16th International Conference on Coastal Engineering. ASCE, pp. 569–587.
- Beji, S., Battjes, J.A., 1993. Experimental investigation of wave propagation over a bar. *Coast. Eng.* 19, 151–162.
- Brocchini, M., Drago, M., Iovenitti, L., 1992. The modelling of short waves in shallow waters: comparison of numerical models based on Boussinesq and Serre equations. Proc. of the 23th Coast. Engng. Conf., Venice, vol. 1. ASCE, Reston, VA, pp. 76–88.
- Canuto, C., Hussaini, M.Y., Quarteroni, A., Zang, T.A., 1987. *Spectral Methods in Fluid Dynamics*. Springer, New York.
- Chen, Y., Liu, P.L.-F., 1995. Modified Boussinesq equations and associated parabolic models for water wave propagation. *J. Fluid Mech.* 288, 351–381.
- Chen, Y., Guza, R.T., Elgar, S., 1997. Modeling spectra of breaking surface waves in shallow water. *J. Geophys. Res.* 102 (C11), 25035–25046.
- Deigaard, R., 1989. Mathematical modelling of waves in the surf zone. Progr. Rep. 69, ISVA, Technical University of Denmark, DK-2800 Lyngby, Denmark, pp. 47–59.
- Eldeberky, Y., Battjes, J., 1996. Spectral modelling of wave breaking: Application to Boussinesq equations. *J. Geophys. Res.* 101 (C1), 1253–1264.
- Elgar, S., Guza, R.T., Raubenheimer, B., Herbers, T.H.C., Gallagher, E.L., 1997. Spectral evolution of shoaling and breaking waves on a barred beach. *J. Geophys. Res.* 102 (C7), 15797–15805.
- Eliassen, E., MACHENHAUER, B., Rasmussen, E., 1970. On a numerical method for integration of the hydrodynamical equations with a spectral representation of the horizontal fields. Technical Report 2. Institut for Teoretisk Meteorologi, University of Copenhagen.
- Fenton, J.D., 1985. A fifth-order Stokes theory for steady waves. *J. Waterw. Port Coast. Ocean Eng.* 111 (2), 216–234.
- Fornberg, B., Whitham, G., 1978. A numerical and theoretical study of certain nonlinear wave phenomena. *Philos. Trans. R. Soc. Lond.*, A 289 (1361), 373–404.
- Freilich, M.H., Guza, R.T., 1984. Nonlinear effects on shoaling surface gravity waves. *Philos. Trans. R. Soc. Lond.*, A 311, 1–41.
- Gobbi, M.F., Kirby, J.T., Wei, G., 2000. A fully nonlinear Boussinesq model for surface waves. Part 2. Extension to $O(kh)^4$. *J. Fluid Mech.* 405, 181–210.
- Herbers, T.H.C., Burton, M.C., 1997. Nonlinear shoaling of directionally spread waves on a beach. *J. Geophys. Res.* 102 (C9), 21101–21114.
- Herbers, T.H.C., Russnogle, N.R., Elgar, S., 2000. Spectral energy balance of breaking waves within the surf zone. *J. Phys. Oceanogr.* 30 (11), 2723–2737.
- Kaihatu, J.M., Kirby, J.T., 1995. Nonlinear transformation of waves in finite water depth. *Phys. Fluids* 7 (8), 1903–1914.
- Kaihatu, J.M., Kirby, J.T., 1998. Two-dimensional parabolic modelling of extended Boussinesq equations. *J. Waterw. Port Coast. Ocean Eng.* 127, 57–67.
- Karambas, T., Koutitas, C., 1992. A breaking wave propagation model based on the Boussinesq equations. *Coast. Eng.* 18, 1–19.
- Kennedy, A.B., Chen, Q., Kirby, J.T., Dalrymple, R.A., 2000. Boussinesq modeling of wave transformation, breaking and runup: I. 1D. *J. Waterw. Port Coast. Ocean Eng.* 126, 39–47.
- Kennedy, A.B., Kirby, J.T., Chen, Q., Dalrymple, R.A., 2001. Boussinesq-type equations with improved nonlinear behaviour. *Wave Motion* 33, 225–243.
- Liu, P.L.-F., Yoon, S.B., Kirby, J.T., 1985. Nonlinear refraction–diffraction of waves in shallow water. *J. Fluid Mech.* 153, 185–201.
- Madsen, P.A., Schäffer, H.A., 1998. Higher-order Boussinesq-type equations for surface gravity waves: derivation and analysis. *Philos. Trans. R. Soc. Lond.*, A 356, 3123–3184.
- Madsen, P.A., Sørensen, O.R., 1992. A new form of Boussinesq equations with improved linear dispersion characteristics. Part 2. A slowly-varying bathymetry. *Coast. Eng.* 18, 183–204.
- Madsen, P.A., Sørensen, O.R., 1993. Bound waves and triad interactions in shallow water. *Ocean Eng.* 20, 359–388.
- Madsen, P.A., Bingham, H.B., Liu, H., 2002. A new Boussinesq method for fully nonlinear waves from shallow water to deep water. *J. Fluid Mech.* 462, 1–30.
- Madsen, P.A., Sørensen, O., Schäffer, H.A., 1997a. Surf zone dynamics simulated by a Boussinesq type model. Part I. Model description and crossshore motion of regular waves. *Coast. Eng.* 32, 255–287.

- Madsen, P.A., Sørensen, O., Schäffer, H.A., 1997b. Surf zone dynamics simulated by a Boussinesq type model. Part II: Surf beat and swash oscillations for wave groups and irregular waves. *Coast. Eng.* 32, 289–320.
- Mase, H., Kirby, J.T., 1992. Hybrid frequency domain KdV equation for random wave transformation. Proceedings of 23rd International Conference on Coastal Engineering, Venice. ASCE, Reston, VA, pp. 474–487.
- Mei, C.C., Ünlüata, Ü., 1972. Harmonic generation in shallow water waves. In: Meyer, R.E. (Ed.), *Waves on Beaches and Resulting Sediment Transport*. Proceedings of an Advanced Seminar Conducted by the Mathematics Research Center, The University of Wisconsin, and The Coastal Engineering Research Center U.S. Army, at Madison. Academic Press, New York.
- Nwogu, O., 1993. An alternative form of the Boussinesq equations for nearshore wave propagation. *J. Waterw. Port Coast. Ocean Eng.* 119, 618–638.
- Orszag, S.A., 1969. Numerical methods for the simulation of turbulence. *Phys. Fluids* 12 (Suppl. III), 250–257.
- Orszag, S.A., 1970. Transform method for calculation of vector coupled sums: application to the spectral form of the vorticity equation. *J. Atmos. Sci.* 27, 890–895.
- Peregrine, D.H., 1967. Long waves on a beach. *J. Fluid Mech.* 27, 815–827.
- Sato, S., Kabling, M.B., Suzuki, H., 1991. Prediction of near-bottom velocity history by a nonlinear dispersive wave model. *Coast. Eng. Jpn.* 35 (1), 67–82.
- Schäffer, H.A., Madsen, P.A., Deigaard, R., 1993. A Boussinesq model for waves breaking in shallow water. *Coast. Eng.* 20, 185–202.
- Scraton, R.E., 1964. Estimation of the truncation error in Runge-Kutta and allied processes. *Comput. J.* 7, 246–248.
- Sørensen, O.R., Schäffer, H.A., Sørensen, L.S., 2004. Boussinesq-type modelling using an unstructured finite element technique. *Coast. Eng.* 50, 181–198.
- Stive, M.J.F., 1980. Velocity and pressure field of spilling breakers. Proc. of the 17th Coastal Engng. Conference.
- Svendsen, I.A., 1984. Wave heights and setup in a surf zone. *Coast. Eng.* 8, 303–329.
- Tao, J., 1983. Computation of wave runup and wave breaking. Internal Report. Danish Hydraulic Institute, DK-2800 Hørsholm, Denmark. 40 pp.
- Ting, F.C., Kirby, J.T., 1994. Observation of undertow and turbulence in a laboratory surf zone. *Coast. Eng.* 24 (1–2), 51–80.
- Veeramony, J., Svendsen, I.A., 2000. The flow in surf-zone waves. *Coast. Eng.* 39, 93–122.
- Wei, G., Kirby, J.T., Grilli, S.T., Subramanya, R., 1995. A fully nonlinear Boussinesq model for surface waves. Part 1. Highly nonlinear unsteady waves. *J. Fluid Mech.* 294, 71–92.
- Zelt, J.A., 1991. Runup of nonbreaking and breaking solitary waves. *Coast. Eng.* 15, 205–246.